Stem Cell Reports
Article
ISSCR
OPEN ACCESS

The trophectoderm acts as a niche for the inner cell mass through C/EBPα-regulated IL-6 signaling

Marcos Plana-Carmona,[1,2] Gregoire Stik,[1,2] Romain Bulteau,[3] Carolina Segura-Morales,[1,2] Noelia Alcázar,[4,5] Chris D.R. Wyatt,[1,2,6] Antonios Klonizakis,[1,2] Luisa de Andrés-Aguayo,[1,2] Maxime Gasnier,[7] Tian V. Tian,[1,2,5] Guillem Torcal Garcia,[1,2] Maria Vila-Casadesús,[1,5] Nicolas Plachta,[7,8] Manuel Serrano,[4,9] Mirko Francesconi,[3] and Thomas Graf[1,2,*]

[1]Gene Regulation, Stem Cells and Cancer Program, Centre for Genomic Regulation (CRG), The Barcelona Institute of Science and Technology (BIST), Barcelona, Spain
[2]Universitat Pompeu Fabra (UPF), Barcelona, Spain
[3]Laboratoire de Biologie et Modélisation de la Cellule, Université de Lyon, ENS, UCBL, CNRS, INSERM, UMR5239, U 1210, 69364 Lyon, France
[4]Institute for Research in Biomedicine (IRB Barcelona), The Barcelona Institute of Science and Technology, Baldiri Reixac 10, 08028 Barcelona, Spain
[5]Vall d'Hebron Institute of Oncology (VHIO), Barcelona, Spain
[6]Department of Genetics, Evolution & Environment, University College London, London, UK
[7]Institute of Molecular and Cell Biology, ASTAR, Singapore, Singapore
[8]Department of Cell and Developmental Biology and Institute for Regenerative Medicine, Perelman School of Medicine, University of Pennsylvania, Philadelphia, PA, USA
[9]Catalan Institution for Research and Advanced Studies (ICREA), 08010 Barcelona, Spain
*Correspondence: thomas.graf@crg.eu
https://doi.org/10.1016/j.stemcr.2022.07.009

SUMMARY

IL-6 has been shown to be required for somatic cell reprogramming into induced pluripotent stem cells (iPSCs). However, how *Il6* expression is regulated and whether it plays a role during embryo development remains unknown. Here, we describe that IL-6 is necessary for C/EBPα-enhanced reprogramming of B cells into iPSCs but not for B cell to macrophage transdifferentiation. C/EBPα overexpression activates both *Il6* and *Il6ra* genes in B cells and in PSCs. In embryo development, *Cebpa* is enriched in the trophectoderm of blastocysts together with *Il6*, while *Il6ra* is mostly expressed in the inner cell mass (ICM). In addition, *Il6* expression in blastocysts requires *Cebpa*. Blastocysts secrete IL-6 and neutralization of the cytokine delays the morula to blastocyst transition. The observed requirement of C/EBPα-regulated IL-6 signaling for pluripotency during somatic cell reprogramming thus recapitulates a physiologic mechanism in which the trophectoderm acts as niche for the ICM through the secretion of IL-6.

INTRODUCTION

In the pre-implantation embryo, totipotent cells segregate into inner cell mass (ICM) cells, which are the *in vivo* source of pluripotent embryonic stem cells (ESCs), and an outer layer of trophectoderm (TE) cells (Zhu and Zernicka-Goetz, 2020; Rossant and Tam, 2022). Alternatively, differentiated cells can be artificially converted into induced pluripotent stem cells (iPSCs) through enforced transcription factor overexpression (Graf, 2011). Single-cell resolution of these reprogramming processes has shown that somatic cells can also diverge from the main path toward pluripotency and that cell-subpopulations appear and activate alternative gene programs, such as the embryonic TE, both *in vitro* (Schiebinger et al., 2019; Liu et al., 2020) and *in vivo* (Abad et al., 2013). In addition, successful iPSC reprogramming has been reported to require interleukin-6 (IL-6) *in vitro* (Brady et al., 2013) and *in vivo* (Mosteiro et al., 2016; Chiche et al., 2017), but how IL-6 and its receptor are regulated and if they play a role in early embryogenesis remains largely unknown.

The *Il6* gene has been described to be activated by C/EBPβ during inflammation (Akira et al., 1990) and cell senescence (Kuilman et al., 2008), while its close relative C/EBPα has been shown to regulate its specific receptor *Il6ra* in newborn hepatocytes (Mackey and Darlington, 2004). In the hematopoietic system, C/EBPα is required for the formation of granulocyte-macrophage progenitors (GMPs) (Zhang et al., 1997) and its overexpression in B cells induces their transdifferentiation into macrophages (Xie et al., 2004). A pulse of C/EBPα in B cells dramatically enhances OSKM-induced reprogramming efficiency (Di Stefano et al., 2014) through the transient generation of GMP-like cells (also called Bα′ cells, Di Stefano et al., 2016). GMPs in turn are the hematopoietic precursor most susceptible to OSKM-induced reprogramming (Eminli et al., 2009; Guo et al., 2014).

Here, we show that the IL-6 pathway is strictly required for the C/EBPα-enhanced reprogramming of B cells into iPSCs and that C/EBPα directly regulates the expression of both the *Il6* and *Il6ra* genes. During early embryo development, C/EBPα is co-expressed with *Il6* in the TE while the receptor is most highly expressed in the ICM. Blocking IL-6 in embryos showed that the cytokine is required for the morula to blastocyst transition, indicating that the TE acts as niche for the ICM through the secretion of IL-6.

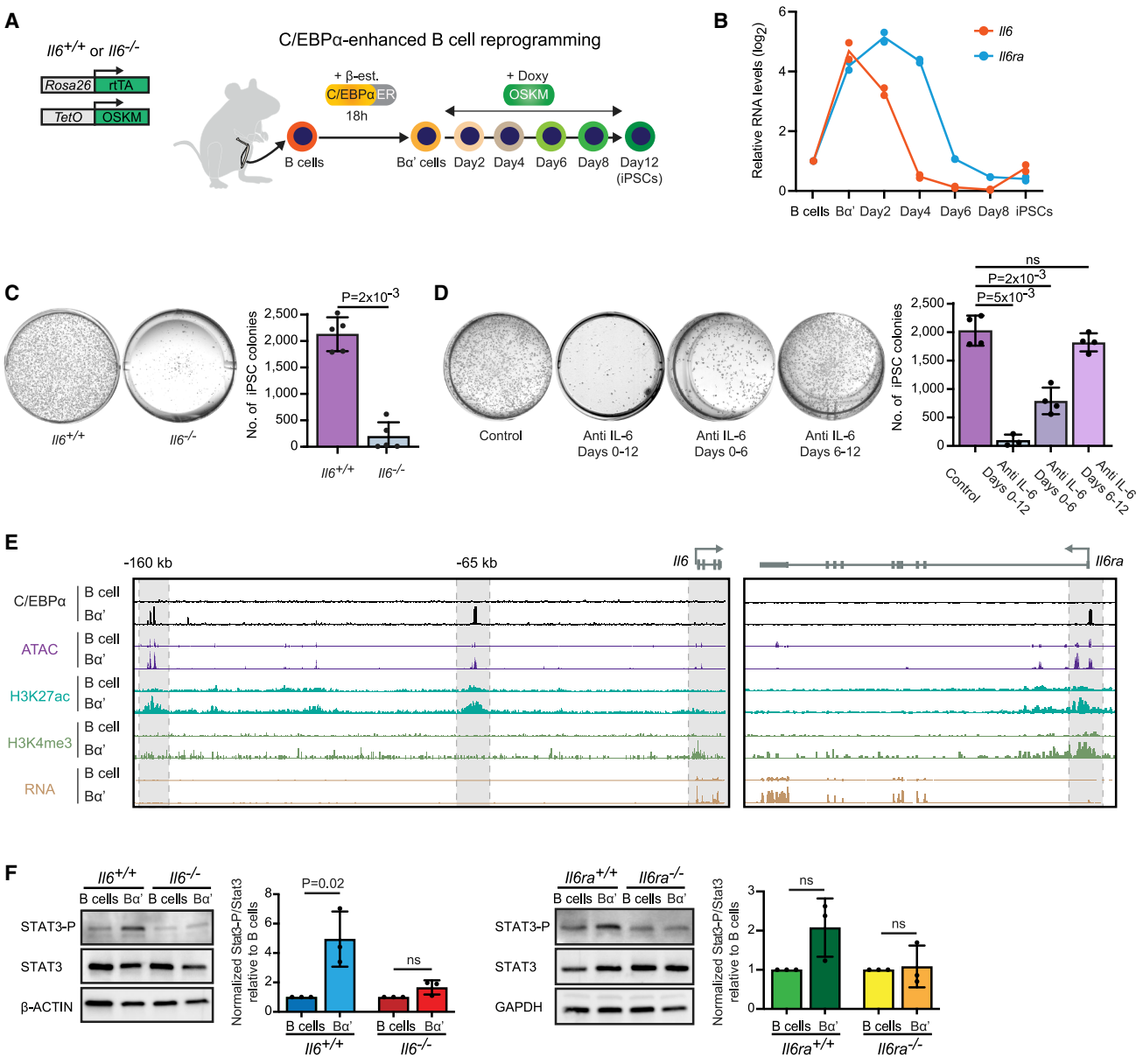

Figure 1. Requirement of IL-6 for C/EBPα-enhanced B cell to iPSC reprogramming and C/EBPα-induced activation of *Il6*

(A) Experimental strategy of C/EBPα-enhanced B cell reprogramming into iPSCs. B cells derived from a reprogrammable mouse strain containing rtTA and a doxycycline (Doxy)-inducible OSKM cassette (Di Stefano et al., 2014) were infected with C/EBPαER, seeded onto MEFs, and induced with β-estradiol (β-est) for 18 h to generate Bα′ cells. After washing out the inducer, Bα′ cells were treated with Doxy for 8 days and scored for alkaline phosphatase-positive (AP+) iPSC colonies at day 12.

(B) *Il6* and *Il6ra* RNA levels during C/EBPα-enhanced B cell reprogramming.

(C) Effect of *Il6* ablation on the number of iPSC colonies, illustrated by images of representative plates and quantification (mean values ± SD, n = 5 biological replicates). Statistical significance was calculated using Student's t test with paired values.

(D) Effect of anti-IL-6 IgG on iPSC reprogramming. Cells were treated daily with 0.1 mg/mL BE0046 antibody, during the whole process (from day 0 to 12), at an early phase (from day 0 to 6), or during later stages (from day 6 to 12). Shown are representative plates with iPSC colonies and quantification (mean ± SD, n = 3 biological replicates for the whole treatment and n = 4 for the other conditions). Statistical significance was determined using one-way ANOVA test with paired values and Dunnett's test for multiple comparisons relative to the control condition (ns, not significant).

(E) Browser screenshots of the *Il6* (left panel) and *Il6ra* (right panel) loci showing C/EBPα binding, chromatin accessibility, histone marks, and gene expression in B and Bα′ cells.

(legend continued on next page)

RESULTS

Il6 ablation blocks B cell to iPSC reprogramming

To study the role of the IL-6 pathway in somatic cell reprogramming we explored our highly efficient C/EBPα-enhanced cell conversion system (Di Stefano et al., 2014). This entails exposing pre-B cells (hereafter called B cells) to C/EBPα for 18 h, generating Bα′ cells, followed by the activation of the Yamanaka factors OCT4, SOX2, KLF4, and MYC (OSKM); (Figure 1A). RNA sequencing (RNA-seq) analysis of samples obtained at various time points showed an approximately 5-fold increase in the expression of *Il6* and *Il6ra* in Bα′ cells with a subsequent decrease of *Il6* at days 2–4 and of *Il6ra* at days 4–6 after OSKM induction (Figure 1B). To test whether the IL-6 pathway is functionally involved in our two-step reprogramming system we tested B cells from $Il6^{-/-}$ mice (Kopf et al., 1994), revealing a 10-fold decrease in the number of iPSC colonies compared with $Il6^{+/+}$ colonies (Figure 1C). Because B cells in these experiments are grown on a feeder layer of inactivated mouse embryonic fibroblasts (MEFs), known to produce IL-6 (Mosteiro et al., 2016), we also tested whether the ablation of *Il6* in the feeders inhibits the reprogramming of B cells. However, the use of $Il6^{-/-}$ MEFs only caused a modest reduction in iPSC colony formation (Figure S1A). The finding that *Il6* and its receptor are most highly expressed between the Bα′ and day 4–6 cell stages (Figure 1B) raised the possibility that IL-6 signaling is predominantly required in the early reprogramming phase. To test this, we added IL-6 neutralizing antibodies from either day 0 to 6 or from day 6 to 12. Cultures treated during the first half of the time course showed an approximately 2.5-fold reduction in iPSC colony numbers, while no significant effect was seen when treated later (Figure 1D). IL-6 neutralization spanning from day 0 to 12 revealed an even stronger inhibitory effect, namely a 10-fold decrease of iPSC colonies, comparable with the reduced numbers observed with $Il6^{-/-}$ B cell cells (Figure 1C).

Our data suggest that C/EBPα-induced B cells themselves produce IL-6 required for B cell to iPSC reprogramming, acting by an autocrine/paracrine mechanism. They also show that IL-6 signaling is only required during the first half of the reprogramming process, consistent with observations made in a reprogramming model with heterokaryons (Brady et al., 2013).

C/EBPα directly regulates *Il6* and *Il6ra* gene expression and activates IL-6 signaling

To study the regulation of the *Il6* gene we analyzed in Bα′ cells binding of C/EBPα by ChIP-seq, chromatin accessibility by ATAC-seq, the enhancer and promoter marks H3K27Ac and H3K4me3 by ChIP-seq, and RNA expression by RNA-seq. C/EBPα was found to bind to −65 and −160 kb sites upstream of *Il6* (Figure 1E, left), which are putative enhancer elements, as indicated by their chromatin accessibility and H3K27ac decoration. Consistent with the observed activation of *Il6* transcripts, its promoter was also decorated with H3K4me3 (Figure 1E, left). In addition, the −65 kb enhancer shows increased contacts with the *Il6* promoter upon C/EBPα overexpression (Figure S1B). In these cells, C/EBPα also binds to the *Il6ra* promoter, where it induces increased chromatin accessibility and decoration with the H3K4me3 and H3K27ac marks, consistent with the observed upregulation of the gene (Figure 1E, right). CEBPA also activates the two genes in the human B cell line BLaER (Stik et al., 2020) (Figure S1C) and the two *IL6* enhancers appear to be evolutionarily conserved since the cells exhibit two CEBPA binding sites at −65 and −150 kb (Figure S1D).

IL-6 signaling is initiated by binding to its specific receptor IL-6RA, which heterodimerizes with IL-6ST (GP130), a signaling chain shared with the leukemia inhibitory factor (LIF) receptor, leading to the phosphorylation of STAT3 and transcriptional activation of downstream targets (Hunter and Jones, 2015). To determine whether C/EBPα overexpression results in activation of STAT3, we performed a western blot of B and Bα′ cell extracts immunostained with phospho-STAT3-specific antibodies. A significant increase of STAT3-P was detected in C/EBPα-induced wild-type but not in $Il6^{-/-}$ Bα′ cells (Figure 1F, left). Similarly, no increased STAT3-P was detected in $Il6ra^{-/-}$ Bα′ cells (Figure 1F, right).

Our data show that C/EBPα directly regulates the expression of the *Il6* and *Il6ra* genes in mouse and human B cells and activates the IL-6 signaling pathway.

The IL-6 pathway is dispensable for C/EBPα-induced B cell to macrophage transdifferentiation

The observed early requirement of IL-6 for B cell reprogramming into iPSCs and high-level expression of *Il6* and *Il6ra* in C/EBPα-induced macrophages (Figures S1E and S1F) raised the possibility that *Il6* ablation likewise affects B cell transdifferentiation into macrophages. We therefore compared the cell conversion kinetics of $Il6^{+/+}$ and $Il6^{-/-}$ B cells, grown on feeders of the corresponding genotype, monitoring by FACS the expression of the B cell marker CD19 and the macrophage marker MAC-1 (CD11b). Knockout and wild-type cells showed insignificant differences in their transdifferentiation kinetics (Figure S1G),

(F) Western blot bands corresponding to STAT3-P and STAT3 obtained from wild-type, $Il6^{-/-}$ and $Il6ra^{-/-}$ B and Bα′ cells. Densitometer-based quantification of β-ACTIN or GAPDH-normalized STAT3-P relative to total STAT3 is shown on the right (mean values ±SD of n = 3 biological replicates). Statistical significance was calculated using Student's t test with unpaired values. See also Figure S1.

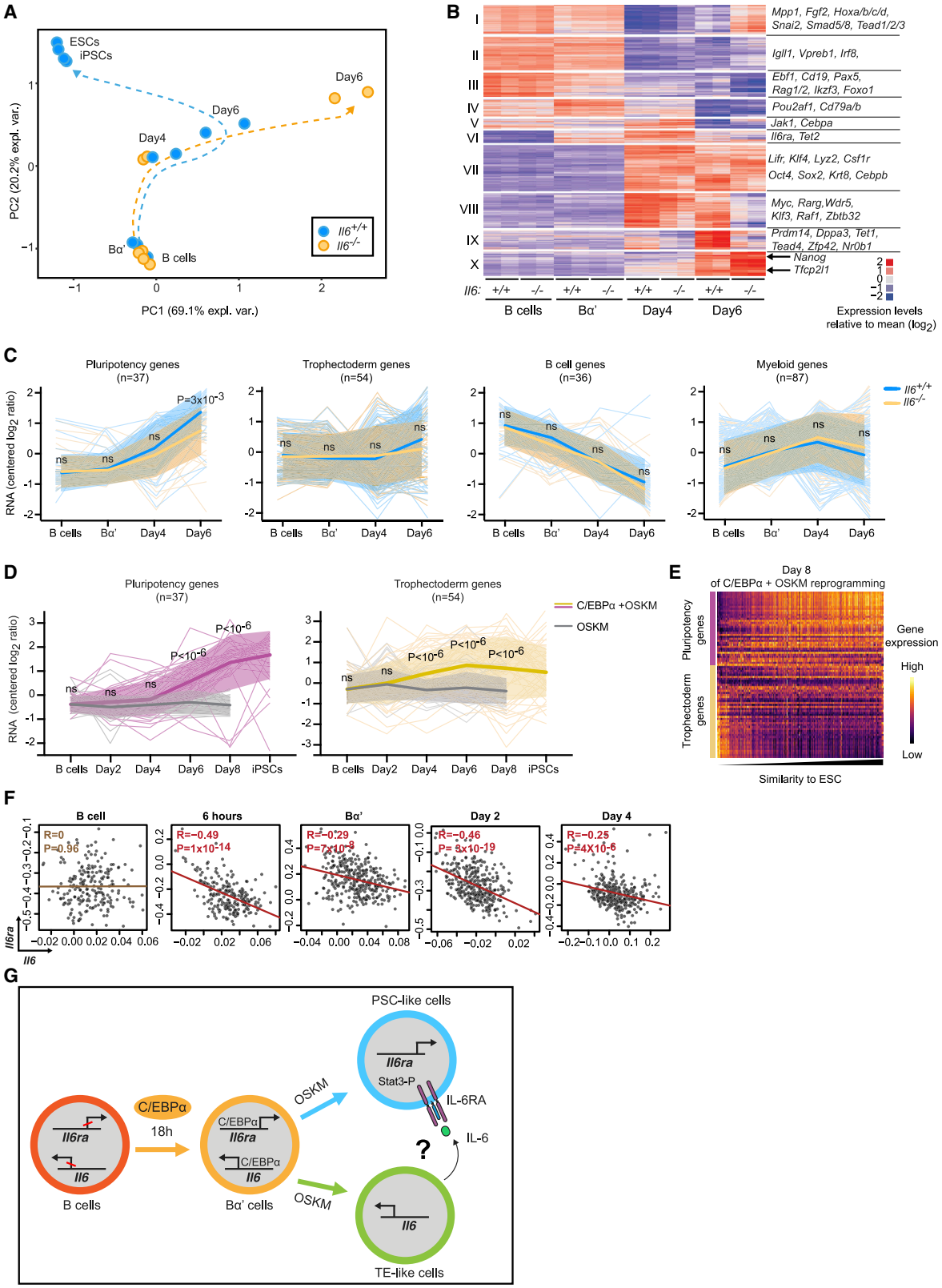

(legend on next page)

and addition of an IL-6 blocking antibody only caused a minor delay in MAC-1 activation (Figure S1H). Of note, macrophages generated in the absence of *Il6* displayed full phagocytic capacity (Figure S1I). These results show that *Il6* ablation does not significantly impair C/EBPα-induced B cell to macrophage transdifferentiation, implying a specific role of IL-6 in the C/EBPα-enhanced reprogramming to iPSCs.

Il6 ablation impairs upregulation of pluripotency-associated genes during reprogramming

To study the mechanism by which IL-6 signaling is required for iPSC reprogramming, we analyzed the impact of *Il6* ablation on gene expression in our C/EBPα-enhanced reprogramming by performing RNA-seq of samples collected at various time points. Principal-component analysis revealed a divergence of the $Il6^{+/+}$ and $Il6^{-/-}$ cell trajectories at days 4–6 of reprogramming (Figure 2A). In addition, the lack of *Il6* led to a significant change in the expression of ~1,000 genes at day 4 and ~4,500 genes at day 6 (Figures S2A and S2B). K-means unsupervised clustering of differentially expressed genes ($p < 0.01$) yielded 10 clusters that fell into 2 major groups, with clusters I to V containing mostly downregulated genes in B cells throughout reprogramming that differed from day 4 onward and clusters VI to X containing mostly upregulated genes (Figure 2B). Genes in cluster I became downregulated by day 4 and re-activated more strongly in $Il6^{-/-}$ cells at day 6. This cluster included the mesenchymal-to-epithelial transition factor genes *Fgf2*, *Snai2*, *Tead1/2/3*, and *Smad5* (Li et al., 2010). Clusters II to V contained downregulated genes and included the B cell genes *Igll1*, *Vpreb1*, *Ebf1*, *Pax5*, and *Cd19*. Clusters VI to IX included upregulated genes encoding the pluripotency-associated factors *Oct4*, *Sox2*, *Myc*, *Prdm14*, *Dppa3*, *Tet1*, *Klf5*, *Zfp42*, and *Nrob1* as well as some TE genes (*Krt8*, *Tead4*, and *Tfap2c*). Finally, cluster X also contained key pluripotency factors like *Nanog* or *Tfcp2l1*, which are specifically downregulated in $Il6^{-/-}$ cells. However, this cluster mostly showed genes upregulated in $Il6^{-/-}$ compared with the wild-type cells, including several laminin and collagen members, such as *Lama4*, *Lamb1*, *Lamc1*, *Col1a1*, *Col3a1*, and *Col5a1*, known to be involved in extracellular matrix formation, as well as BMP signaling genes (e.g., *Bmp1*, *Bmp2*, and *Bmp6*). These findings raise the possibility that some $Il6^{-/-}$ intermediates may acquire identities that differ from the pluripotency phenotype.

Next, we determined the reprogramming kinetics of a group of signature genes characteristic for different lineage-restricted gene expression programs. This showed that the lack of *Il6* impaired the upregulation of pluripotency genes, most notably at day 6, and mildly affected TE genes ($p = 0.07$ at day 6, Figure 2C). In addition, cell-cycle-associated genes were significantly impaired in knockout cells at day 6, probably reflecting their reduced proliferation compared with reprogrammed $Il6^{+/+}$ cells (Figure S2C). In contrast, *Il6* ablation did not appreciably affect the silencing of B cell signature genes or the upregulation of myeloid genes (Figure 2C). Examples of individual genes representative for each of these categories are shown in Figure S2D.

The observation that both PSC- and TE-associated genes become upregulated during C/EBPα-enhanced reprogramming (Figure 2D) raised the question whether this reflects the formation of distinct cell subpopulations or cells with mixed phenotypes. We therefore plotted the RNA levels

Figure 2. *Il6* deficiency impairs the upregulation of pluripotency genes during reprogramming

(A) Principal-component analysis (PCA) of gene expression dynamics of 38,019 genes during reprogramming *of* $Il6^{+/+}$ and $Il6^{-/-}$ B cells, showing biological duplicates and average trajectories.

(B) Heatmap of unsupervised K-means clustering of genes differentially expressed between $Il6^{+/+}$ and $Il6^{-/-}$ cells ($p < 0.01$) at different times during reprogramming, showing biological duplicates. Representative examples of genes within each cluster are shown on the right.

(C) Gene expression changes (RNA-seq) of pluripotency, trophectoderm, B cell, and myeloid signature genes during reprogramming of $Il6^{+/+}$ and $Il6^{-/-}$ B cells. Thin lines represent average values of biological duplicates for each gene, thick lines the mean and shades the SD. Statistically significant differences between $Il6^{+/+}$ and $Il6^{-/-}$ cells are indicated by p values determined using two-way ANOVA and Šídák's multiple comparison tests (ns, not significant). Signature genes are listed in Table S1.

(D) Expression kinetics (RNA-seq) of pluripotency and trophectoderm signature genes, comparing C/EBPα pulsed B cells (C/EBPα + OSKM) with non-pulsed cells (OSKM) (RNA-seq by Di Stefano et al., 2014). Lines represent average values of biological duplicates for each gene, centered around a thicker mean line for the whole signature and shades denoting SD. Statistical significance is determined using two-way ANOVA and Šídák's multiple comparison tests. Signature genes are listed in Table S1.

(E) Heatmap of pluripotency and trophectoderm signature genes' expression obtained from single cells at day 8 of reprogramming (Francesconi et al., 2019), with values of individual cells ordered according to their similarity to ESCs.

(F) Correlation plots between *Il6ra-Il6* gene expression pairs in single cells at various time points during reprogramming. Pearson's correlation coefficients (R), p values (P), and tendency lines are depicted in each plot. Correlation coefficients are color coded in brown and red, respectively, corresponding to zero and negative values.

(G) Model of the role of C/EBPα and the IL-6 pathway during the C/EBPα-enhanced reprogramming of B cells into pluripotent and TE-like cells. See also Figure S2.

of pluripotency and TE signature genes of day 8 induced cells in comparison with that of ESCs, using a single-cell gene expression dataset (Francesconi et al., 2019). The observed inverse correlation between the expression of PSC- and TE-associated genes (Figure 2E) suggests a segregation into distinct subpopulations, despite a large degree of variability at the single-cell level. Similarly, we explored whether the ligand-receptor expression between the initially upregulated *Il6* and *Il6ra* (Figure 1B) also corresponded to distinct populations. For that, we pairwise correlated the expression levels of *Il6* and *Il6ra* from B cells to day 4, around which their expression drops. After the pulse of C/EBPα, *Il6* and *Il6ra* start to negatively correlate and this is maintained until day 4, suggesting that cells predominantly express either *Il6* or *Il6ra* already at an early time point (Figure 2F).

Our data are compatible with the notion that IL-6 is required in a paracrine fashion among B cells for the robust upregulation of pluripotency genes, while having a minor effect on the upregulation of TE genes. They also suggest that, during C/EBPα-enhanced reprogramming, pluripotent-like cells segregate from TE-like cells (Figure 2G).

Cebpa and *Il6* are co-expressed in the TE while *Il6ra* is predominantly expressed in the ICM

The finding that C/EBPα-enhanced iPSC reprogramming requires IL-6 and that both *Il6* and *Il6ra* genes are regulated by C/EBPα raised the possibility that the C/EBPα-IL-6 axis is also involved in embryo development (Figure 3A). We therefore analyzed RNA-seq datasets of mouse pre-implantation embryos when totipotent cells first differentiate into pluripotent (ICM) and TE layers (Deng et al., 2014; Guo et al., 2010). This showed that, within the mouse blastocyst, both *Cebpa* and *Il6* are selectively expressed in the TE while *Il6ra* expression is enriched in the ICM (Figure 3B). Likewise, within developmentally earlier morula stage embryos, *Cebpa* was enriched in the outer-layer cells of morulas along with the TE markers *Gata3* and *Krt8*, whereas inner-layer cells were enriched for *Nanog* and *Sox2* expression (Figures S3A and S3B).

Strikingly, the observed gene expression pattern is evolutionarily conserved, as revealed by our analysis of human blastocyst single-cell data (Petropoulos et al., 2016). *CEBPA* and *IL6* are co-expressed within the TE while *IL6RA* is enriched in the ICM, as validated by the expression of lineage markers (Figures 3C and S3C). Of note, none of *CEBPB*, *CEBPD*, or *CEBPE* showed an enrichment in the TE (Figure S3D). Resolving the ICM of E5.5 human blastocysts into epiblast and primitive endoderm cells, showed that *IL6RA* expression is significantly higher in both ICM layers than in TE cells (Figure S3E). A similar but slightly less pronounced selective expression pattern of these three markers was also observed in E6.5 blastocysts (Figure S3F). Since TE cells can be subdivided into polar and mural subsets (Gardner, 2000), we also analyzed existing datasets for the distribution of our genes of interest. While coverage of *Il6* expression in mouse embryos (Nakamura et al., 2015) was insufficient, human blastocysts showed a significant enrichment of *IL6* and *CEBPA* expression in the polar TE subpopulation of E6.5 and E7.5 blastocysts, although less pronounced than the polar TE marker *CCR7* (Figure 3D). Similarly, mouse blastocysts stained with an antibody against C/EBPα revealed strong expression in the TE, both in polar and mural areas (Figure 3E).

It has been reported that human ESCs can be induced to differentiate into TE-like cells using two experimental approaches. In the first, hESCs were treated with BMP4 (Krendl et al., 2017); in the second, naive hESCs were exposed to a combination of the MEK inhibitor PD0325901 and the TGF-β inhibitor A-83-01 (PD + A83) (Guo et al., 2021). In both TE differentiation strategies, *CEBPA* and *IL6* become upregulated while *IL6RA* becomes downregulated (Figures 3F and 3G). As expected, *GATA3* and *KRT8* were upregulated and *NANOG* and *SOX2* downregulated (Figures 3F and 3G), validating the described hESC to TE conversion.

These results show that *CEBPA* and *IL6* are co-expressed in TE cells and that *IL6RA* is mostly expressed in the ICM in both mice and humans. The observed upregulation of *CEBPA* and *IL6* and downregulation of *IL6RA* during the induced differentiation of hESCs into TE cells further supports the selective expression of the IL-6 pathway genes within the first two blastocyst lineages.

Perturbation experiments of C/EBPα in ESCs and in embryos alter the expression of IL-6 signaling genes

The observed expression of *Cebpa* and *Il6* in the blastocyst TE *in vivo* and in hESC-derived TE-like cells *in vitro* raised the possibility that the factor could regulate *Il6* expression in ESCs and during embryo development as in B cells. To test this idea, we monitored the effect of C/EBPα overexpression in ESCs. For this purpose, we generated two stable, tamoxifen-inducible E14 ESC clonal lines expressing C/EBPαERT2-dTomato. These cells were treated for 12 and 48 h with tamoxifen and subsequently analyzed by RNA-seq, revealing an approximately 4-fold upregulation of *Il6* and ~30-fold of *Il6ra* (Figure 4A). Of note, the *Il6ra* levels in the induced cells were ~250 times higher than those of *Il6*. To determine whether C/EBPα also induces the expression of IL-6 genes in human ESCs, we analyzed an RNA-seq dataset of a human ESC line expressing a doxycycline-inducible form of CEBPA, before and after a 48 h treatment with doxycycline (Nakatake et al., 2020). Here again the treated cells showed an approximately 2-fold upregulation of *IL6* and approximately 4-fold upregulation of *IL6RA* as well as similar differences in their initial expression levels

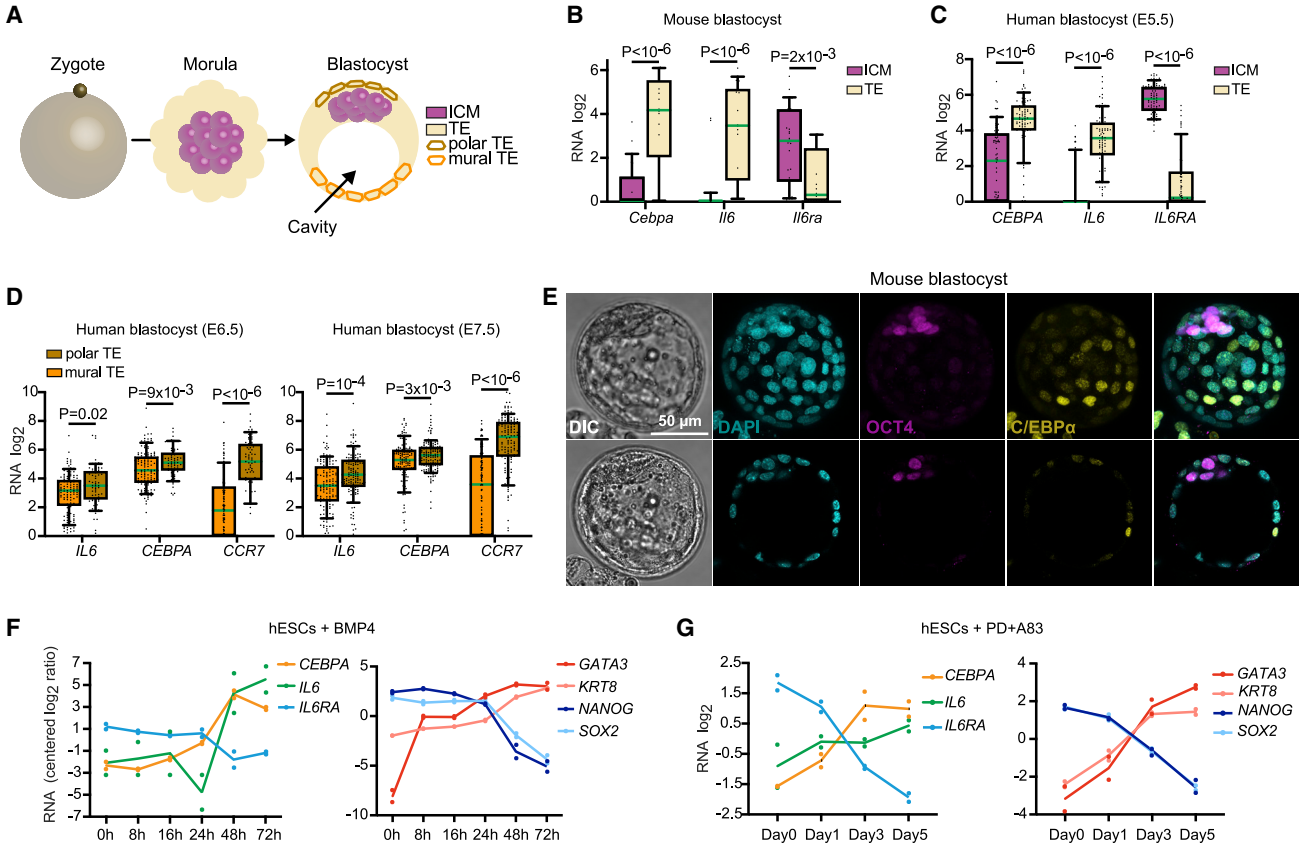

Figure 3. *Cebpa* and *Il6* expression are enriched in the TE while *Il6ra* is enriched in the ICM

(A) Diagram depicting the segregation of the TE from the ICM layer during the morula to blastocyst transition.

(B) *Cebpa*, *Il6*, and *Il6ra* expression levels in the TE and ICM of mouse blastocysts by single-cell RNA-seq (Deng et al., 2014). Dots represent gene expression values of single cells in the ICM and TE, green lines represent median values, and boxplots and whiskers represent 90th and 10th percentiles, respectively. Statistical significance was determined using multiple unpaired Student's t test applying Benjamin, Kieger, and Yekutieli's correction methods. Ns, not significant. For the ICM group, only cells with >0 *Il6ra* RPKMs were selected (n = 28/35, 80%); in the TE group, only cells with >0 *Il6* RPKMs (n = 16/57, 28%).

(C) As in (B), but for human blastocysts [Petropoulos et al., 2016]). The values shown for the ICM correspond to a combination of epiblast (Epi) and primitive endoderm (PrE) cells. For the ICM group, all cells showed >0 *Il6ra* RPKMs; in the TE group, only cells with >0 *Il6* RPKMs were selected (n = 78/142, 54.9%).

(D) Expression distribution of *CEBPA*, *IL6*, and *CCR7* in single mural and polar TE cells from human blastocysts. Only cells with >0 *Il6* RPKMs were selected (n = 185/331, 55.9% in E6.5, and n = 273/388, 70.3% in E7.5).

(E) Immunofluorescence images (3D projections and single z-planes) of C/EBPα and OCT4 in a mouse blastocyst (bright field in DIC). OCT4 stains pluripotent ICM cells. DNA was stained with DAPI.

(F) Kinetics of *CEBPA*, *IL6*, *IL6RA*, *GATA3*, *KRT8*, *NANOG*, and *SOX2* gene expression during induced TE differentiation after BMP4 addition to hESCs (RNA-seq by Krendl et al., 2017).

(G) Kinetics of *CEBPA*, *IL6*, *IL6RA*, *GATA3*, *KRT8*, *NANOG*, and *SOX2* gene expression during induced TE differentiation after PD + A83 addition to hESCs (RNA-seq by Guo et al., 2010). See also Figure S3.

in hESCs (Figure 4B). To determine whether another TE-associated transcription factor is able to upregulate these genes in human ESCs, we analyzed the same dataset (Nakatake et al., 2020) for the effect of GATA3 overexpression. This revealed an approximately 3-fold upregulation of *IL6*, similar to that observed for CEBPA. However, GATA3 only induced a modest (~1.5-fold) activation of the *IL6RA* gene (Figure S4A, left). Curiously, also CEBPB strongly upregulates *IL6RA* (~9-fold) but not *IL6* expression in the hESCs context (Figure S4A, right).

We next studied the impact of *Cebpa* ablation in cultured embryos. Since $Cebpa^{-/-}$ mice die perinatally (Wang et al., 1995), we crossed heterozygous animals, yielding $Cebpa^{-/-}$, $Cebpa^{+/-}$, and $Cebpa^{+/+}$ zygotes. Isolated zygotes were cultured for 2.5 and 4.5 days, reaching morula and blastocyst stages, respectively (Figure 4C). A total of 21 morulas and 24

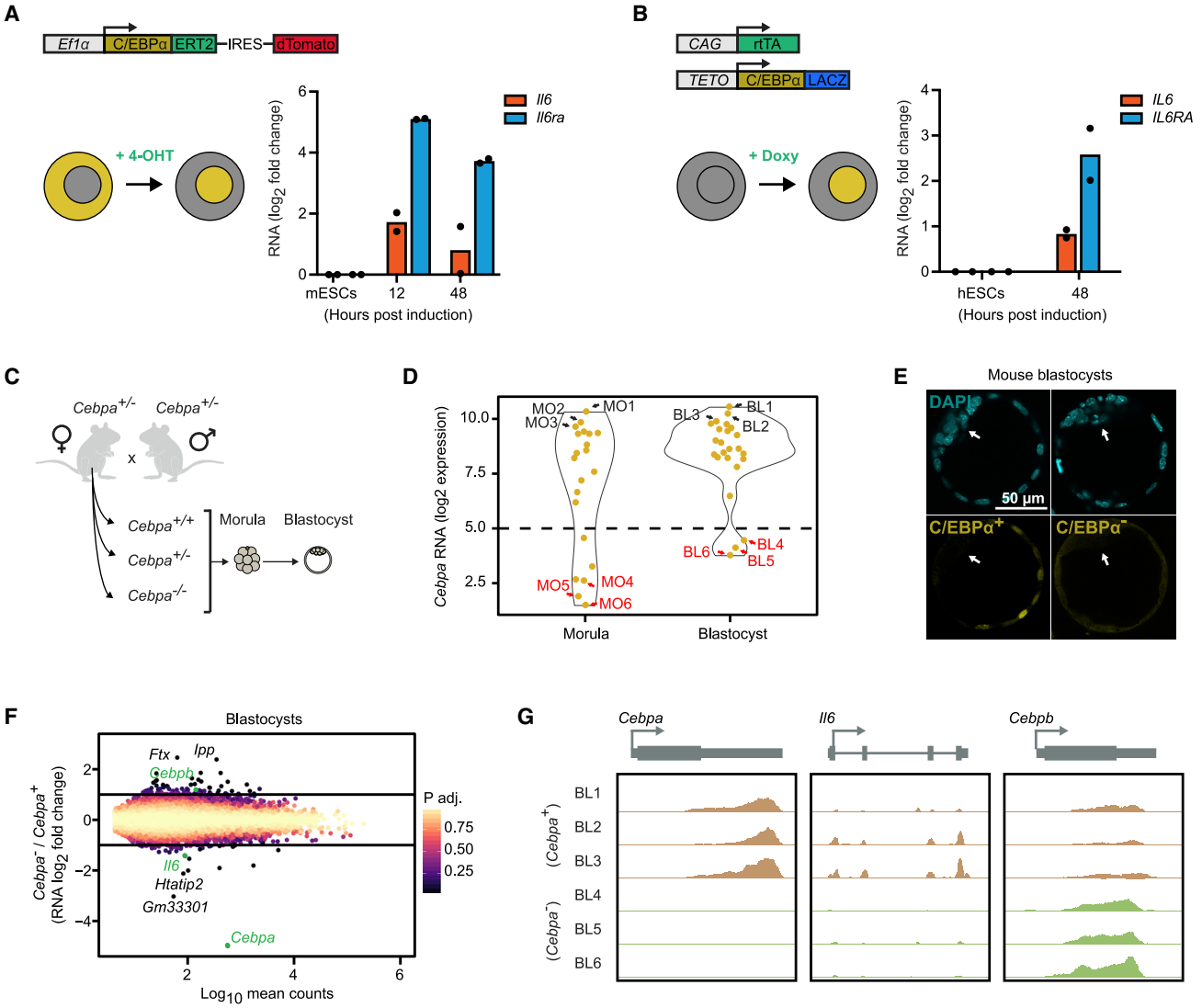

Figure 4. Effect of *Cebpa* overexpression in ESCs and ablation in cultured blastocysts

(A) Overexpression of C/EBPα in murine ESCs, showing the construct used, schematics of induction, and gene expression changes for *Il6* and *Il6ra* after 12 and 48 h.

(B) As in (A), but for human ESCs and only after 48 h.

(C) Experimental strategy to study the impact of *Cebpa* ablation on early mouse development. Zygotes from an F1 cross of $Cebpa^{+/-}$ mice were placed in culture and harvested at the 8- to 16-cell morula (n = 21) and blastocyst stage (n = 24) for RNA-seq analyses.

(D) *Cebpa* expression in the morulas and blastocysts obtained from the F1 cross. The dashed line sets the threshold between $Cebpa^{-}$ and $Cebpa^{+}$ embryos. The top three $Cebpa^{-}$ and $Cebpa^{+}$ embryos, highlighted by black and red arrows, were selected for more detailed analyses.

(E) Immunofluorescence images (z-planes) of C/EBPα in mouse blastocysts derived from an F1 cross of $Cebpa^{+/-}$ mice. DNA was stained with DAPI and white arrows indicate ICM regions.

(F) Volcano plots of genes differentially expressed in the selected $Cebpa^{-}$ and $Cebpa^{+}$ embryos at the blastocyst stage. Genes above or below the two lines differ significantly ($p < 0.05$).

(G) Browser screenshots showing RNA expression of *Cebpa*, *Il6*, and *Cebpb* genes for the selected $Cebpa^{-}$ and $Cebpa^{+}$ blastocysts. See also Figure S4.

blastocysts were subjected to RNA-seq analyses, allowing to distinguish $Cebpa^{-}$ and $Cebpa^{+}$ embryos (Figures 4D and S4B), also detectable at the protein level (Figure 4E). At the morula stage, six embryos were found to be $Cebpa^{-}$, closely matching the 5.25 embryos expected from Mendelian ratios. In contrast, at the blastocyst stage, three $Cebpa^{-}$ blastocysts

were detected instead of the expected six (Figure 4D). To analyze the impact of *Cebpa* on gene expression, we selected the top 3 *Cebpa*$^{-}$ and *Cebpa*$^{+}$ embryos. At the morula and blastocyst stages 27 and 32 genes, respectively, showed a significantly altered expression between the *Cebpa*$^{-}$ and the *Cebpa*$^{+}$ groups (Figures 4F and S4C). Remarkably, in blastocysts, *Il6* was among the differentially expressed genes, showing a reduced expression in *Cebpa*$^{-}$ ($p = 0.048$). This was accompanied by a compensatory upregulation of *Cebpb* (Figure 4G), while *Cebpe* and *Cebpd* remained unchanged as did *Il6ra* (Figure S4D). Finally, *Cebpa* also showed a modest positive correlation with *Il6* expression and that of the TE marker *Gata3* when analyzing all 24 blastocysts, while it showed a negative correlation with *Il6ra* expression and the ICM marker *Oct4*. No correlation was found at the morula stage (Figure S4E).

Together, our experiments show that overexpression of C/EBPα upregulates both *Il6/IL6* and *Il6ra/IL6RA* genes in mouse and human PSCs. Moreover, *Cebpa* is required for *Il6* expression in mouse blastocysts and it is non-redundant with *Cebpb* at this developmental stage.

Blastocysts secrete IL-6 and blocking antibodies delay the morula to blastocyst transition

Our data described so far are consistent with the notion that IL-6 secreted by TE cells in blastocysts signals to the receptor expressed in ICM cells. This notion is in line with a report describing that IL-6 blocking antibodies reduce STAT3 phosphorylation in blastocysts (Do et al., 2013). To directly demonstrate IL-6 secretion during embryo development, we cultured pools of 30 zygotes each for 1.5–4.5 days to obtain two- to four-cell embryos, morulas, and blastocysts. Using an ELISA assay, we detected ~2 pg/mL IL-6 in the two- to four-cell stage embryo and morula pools and ~10 pg/mL of IL-6 in the blastocyst pool (Figure 5A), consistent with *Il6* mRNA expression in blastocysts (Figure 3B). We next determined whether the observed IL-6 secretion and the reported IL-6 signaling (Do et al., 2013) has a physiological role. For this purpose, we established embryo cultures in the presence of an IL-6 blocking IgG or an isotype-matched IgG against horseradish peroxidase used as a control. Microscopic examination of the embryos up to day 2.5 showed no differences in their development. However, at day 3.5, we observed a significantly lower proportion of embryos exhibiting a cavitation in the anti-IL-6-treated cultures, indicative of an impaired formation of early blastocysts. A slight cavitation impairment persisted at day 4.5 blastocysts (Figures 5B and 5C). Conversely, adding recombinant IL-6 in the medium of *in-vitro*-cultured porcine embryos has been reported to induce STAT3 activation and to enhance parthenote development (Shen et al., 2012).

In sum, our results show that cultured blastocysts secrete significant amounts of IL-6, likely produced by TE cells. The finding that neutralizing IL-6 caused a delay in the morula to blastocyst transition indicates that the IL-6 pathway is physiologically relevant for pre-implantation embryo development in mouse.

Exogenous IL-6 binds to the ICM region in blastocysts exposed to an IL-6 reporter protein

The experiments described so far suggest that, during the morula to blastocyst transition, IL-6 secreted by the TE signals to the ICM. However, attempts to directly visualize IL-6 binding in the embryo by IL-6 and IL-6RA immunostaining failed. As an alternative, we engineered an IL-6-Emerald fusion construct to identify binding of fluorescent IL-6 to the surface of IL-6RA-expressing cells. First we confirmed that soluble IL-6-Emerald protein binds to the surface of 293T cells (which are known to express the IL-6 receptor [Von Laue et al., 2000]), while no signal was observed in embryos treated with condition medium from control cells (Figure S5A). We then proceeded to perform the embryo experiments, by incubating blastocysts with soluble IL6-Emerald protein for 30 min, staining the live embryos with Hoechst and analyzing them by confocal microscopy. The images obtained revealed the selective localization of the Emerald signal to the ICM area (Figure 5D) and in a similar patchy pattern as observed upon its overexpression in embryos (Figure S5B). These findings directly show that IL-6 binds selectively to the ICM region, in line with the RNA-seq experiments showing an enrichment of *Il6ra* expression in the ICM (Figure 3B). In addition, the ICM localization of IL-6-Emerald in mouse embryos further complements the observed increase in the number of ICM cells in bovine blastocysts cultured with recombinant IL-6 (Wooldridge and Ealy, 2019), which suggested that ICM cells might be the functional targets expressing the IL-6 receptor.

DISCUSSION

Here, we describe that IL-6 signaling is strictly required for C/EBPα-enhanced reprogramming of B cells into iPSCs but not for their transdifferentiation into macrophages. In this context, C/EBPα binds to both *Il6* and *Il6ra* genes and activates their expression. In the developing embryo, we find that the TE co-expresses *Cebpa* and *Il6*, while the receptor is preferentially expressed by the ICM, in both mouse and human. On the other hand, whether the cells that initially upregulate *Il6* or *Il6ra* turn respectively into the TE- and PSC-like cells during reprogramming (tallying the embryo situation as is speculated in Figure 2G) remains unresolved. Our finding that C/EBPα regulates the expression of *Il6* in the TE layer of blastocysts indicates that the TE may act as a niche for the ICM through the secretion of IL-6

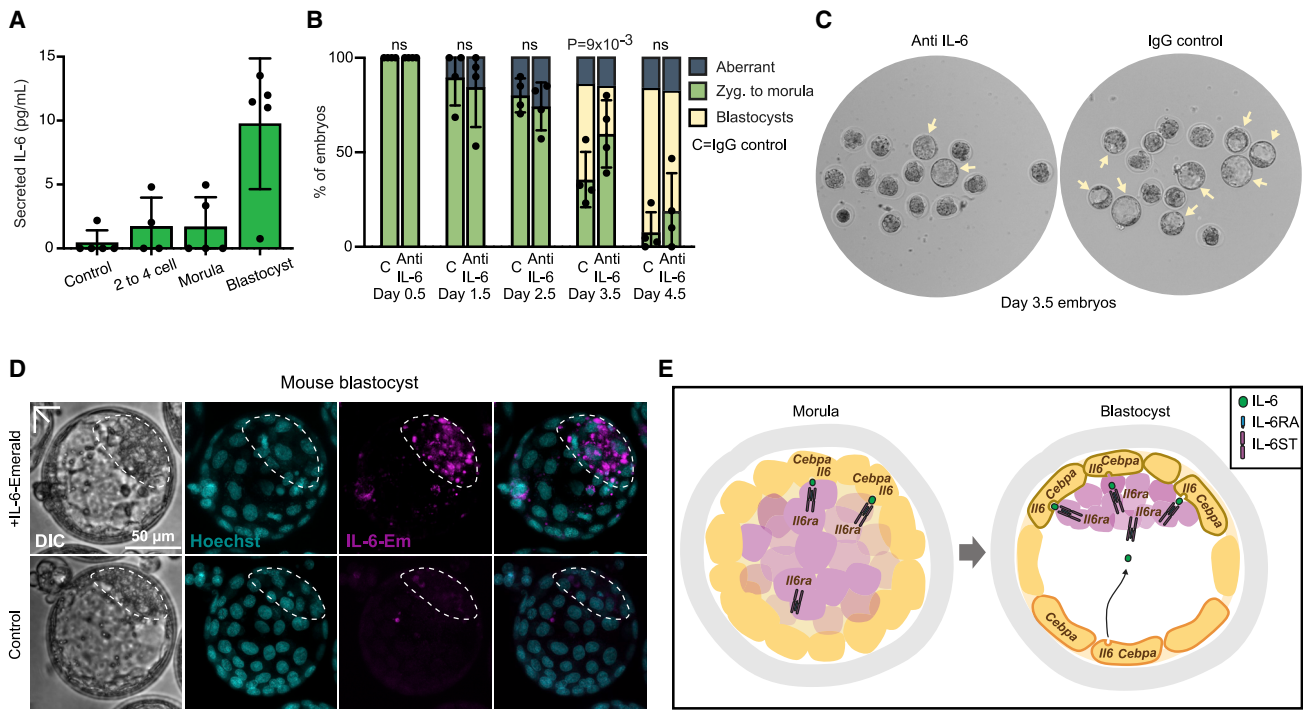

Figure 5. Effect of IL-6 neutralization on blastocyst formation and visualization of IL-6 binding

(A) Detection of IL-6 by an ELISA assay in embryos at different developmental stages. Each sample tested contained a pool of 30 embryos placed in 30 µL of culture medium. Mean values ± SD of results obtained from five separate experiments. Control, culture medium.

(B) Quantification of the effect of IL-6 blocking antibody on the formation of blastocysts. Results were obtained with 245 embryos treated with anti-IL-6 and 208 embryos with control IgG (against horseradish peroxidase) in 4 experiments. Statistical significance was determined by multiple paired Student's t test applying Holm-Šídák's correction method. Ns, not significant.

(C) Images of embryos cultured for 3.5 days with an anti-IL-6 or control IgG. Yellow arrowheads pinpoint embryos identified as blastocysts by the formation of a blastocoel cavity.

(D) Visualization of IL-6 binding. Images of a blastocyst incubated with the supernatant of IL-6-Emerald-transfected 293T cells (top) or of a non-transfected culture (bottom). White dashed lines indicate the ICM regions. DNA was stained using 1 µg/mL Hoechst 33342 (blue). IL-6-Emerald is shown in purple. Similar findings were made with a total of seven embryos.

(E) Model of how C/EBPα-induced IL-6 produced by TE cells could engage in a crosstalk with the receptor expressed in the ICM during the early morula to late blastocyst transition. ICM cells are shown in pink, TE cells in yellow. Zona pellucida is the outer layer depicted in gray, fully permeable to IgG and IgM immunoglobulins (Sellens and Jenkinson, 1975). See also Figure S5.

(Figure 5E), recapitulating our observations for such regulatory axis during B cell to iPSC reprogramming. This adds to the growing list of factors that have been described to engage in a pre-implantation embryo crosstalk, including FGF4, BMP4, IL-11, Nodal, and WNT6/7B (Zhu and Zernicka-Goetz, 2020; Rivron et al., 2018). It is possible that the reason why the IL-6 crosstalk has not been reported before is that it was obscured by LIF, which is added during experimental approaches to study the requirement of soluble factors, such as during blastoid formation (Rivron et al., 2018). In addition, the fact that *Lif* is expressed before *Il6* during pre-implantation embryo development, at the two- to four-cell stage (Do et al., 2013), supports the notion that IL-6 and not LIF is the cytokine critical for blastocyst formation. Similarly, *LIF* is expressed at very low levels and before *IL6* in human embryos (Bourillot et al., 2020), raising the possibility that IL-6 signaling at this early stage of life is evolutionarily conserved.

Our previous work has shown that the ability of C/EBPα and the closely related factor C/EBPβ to enhance OSKM-induced reprogramming of B cells is not shared with unrelated factors capable of inducing transdifferentiation, such as with the erythroid, muscle, and neuronal fate inducing factors GATA1, MYOD, and ASCL1, respectively (Di Stefano et al., 2014). In addition, among C/EBP family members, C/EBPα uniquely shows a TE-specific expression in mice and humans and is non-redundantly required for *Il6* expression. Moreover, the observed compensatory upregulation of *Cebpb* in *Cebpa* knockout embryos does not prevent a reduction in *Il6* expression. We therefore speculate that, in TE cells, C/EBPα specifically interacts with another TE-associated co-factor(s) to upregulate *Il6* but not *Il6ra*.

It is puzzling that C/EBPα upregulates *Il6ra* in PSCs and in a subset of B cells, but that the receptor is not expressed in TE cells. This might be explained by the presence in the former cell types of a C/EBPα co-factor(s) required for *Il6ra* expression not present TE cells. It also suggests that, in the ICM, *Il6ra* falls under the control of alternative factors. Future experiments are needed to address the question whether IL-6 signaling is not only required for the high-level activation of pluripotency genes during reprogramming, as described here, but also for the formation of the ICM during embryo development. The IL-6-mediated crosstalk between the TE and ICM described here extends the many known functions of IL-6 in adult tissues to the earliest cell fate decision in vertebrate development.

EXPERIMENTAL PROCEDURES

C/EBPα-enhanced reprogramming of B cells into iPSCs

Reprogramming of primary B cells from wild-type or *Il6*$^{-/-}$ reprogrammable mice was performed as described previously (Di Stefano et al., 2014, 2016). In brief, freshly isolated B cells were infected with C/EBPα-ER-hCD4 retrovirus and hCD4-positive cells were plated at 500 cells/cm^2 in gelatinized 12-well plates onto wild-type or *Il6*$^{-/-}$ inactivated MEF feeders in 20%-FBS RPMI medium with 10 ng/mL IL-7. The transcription factor was shuttled into the nucleus by the addition of 100 nM β-estradiol for 18 h. After β-estradiol washout, the cultures were switched to N2B27 medium (50% DMEM-F12 [12634010, Gibco], 50% neurobasal [21103049, Gibco], 100× N2 supplement [17502048, Gibco], and 50× B27 supplement [17504044, Gibco]) and addition of 10 ng/mL IL-4 (217-14, Preprotech, 10 ng/mL IL-7, and 2 ng/mL IL-15 [210-15, Preprotech]). The final culture medium also contained 100× MEM non-essential amino acid solution (11140068, Gibco), 1 mM sodium pyruvate (11360070, Gibco), 100 U/mL penicillin-100 ng/mL streptomycin, 2 mM L-glutamine, and 0.1 mM 2-mercaptoethanol.

The OSKM expression was activated by the addition of 2 μg/mL doxycycline (D9891, Sigma). Samples needed for western blots or RNA-seq were harvested by trypsinization followed by removal of feeder cells through differential adherence to tissue culture dishes for 40 min. iPSC colony formation was assessed at the end of the process by alkaline phosphatase staining as detailed below.

Anti-IL-6 blocking treatments were performed by adding 0.1 mg/mL of IgG1 the antibody BE0046 (BioXCell) to the cultures. For rescue experiments, an additional 20 ng/mL of mouse recombinant IL-6 protein (406-ML, R&D Systems) was added. Both neutralization and rescue experiments consisted in adding the compounds daily from the pulse of C/EBPα until the end of reprogramming.

Scoring and counting of iPSC colonies

Induced reprogrammable B cells were cultured in 12-well plates containing feeders MEFs and analyzed at day 12 after OSKM induction. Cultures were washed twice with 0.05% PBS-Tween 20 (PBSTw), fixed for 2 min in 4% PFA and washed once again in 0.05% PBSTw. Cells were then incubated in freshly prepared alkaline phosphatase staining solution at room temperature in the dark for 10–20 min and washed twice in PBS. Alkaline phosphatase expression was detected by the purple color of the iPSC colonies. Plates were scanned (Perfection V850 Pro, Epson) and colonies were counted in Fiji software. See Table S3 for iPSC staining solution composition.

Pre-implantation mouse embryo cultures

Zygotes were collected from the ampulla and cumulus cells removed by incubation with 300 μg/mL hyaluronidase (H4272, Sigma) in M2 medium (M7167, Sigma). After washing the embryos in a few drops of KSOM medium (MR-106-D, Millipore), they were cultured in KSOM microdrops under mineral oil (NO-400K, Nidacon) in an incubator with 5% CO_2 at 37°C. Embryos were handled with a mouth aspirator (A5177-5EA, Sigma) coupled to fire-polished glass Pasteur pipettes and collected at different stages of development from the *in vitro* cultures either for RNA-seq or protein immunostaining as detailed in the sections below. To track their development in control or IL-6 blocking conditions, phase contrast pictures of the developing embryos were taken with a Leica inverted microscope (DMI6000B) and embryos were counted using Fiji software.

The amounts of IL-6 produced by the various samples was assessed using an ELISA kit (M6000B, R&D Systems) according to the manufacturers' instructions. Emissions of the samples at 450 nm wavelength were measured in a plate reader (SPECTROstar Nano, BMG Labtech). Anti-IL-6 blocking treatments were performed by adding 0.1 mg/mL of antibody (BE0046, BioXCell) IgG1 or anti-horseradish peroxidase antibody (BE0088, BioXCell) IgG1 as a control in culture microdrops from the zygote stage up to late blastocysts.

Protein immunostaining

Embryos were fixed in 4% PFA for 10 min at room temperature. They were then washed twice in PBS for 5 min before permeabilization with 0.5% Triton X-100 PBS (0.5% PBST). Zygotes to morulas were permeabilized for 10 min while blastocysts were permeabilized for 15 min. Embryos were washed twice in 0.1% PBST for 5 min before incubation in 0.1% PBST containing 3% BSA (9048-46-8, Sigma) for 45 min at room temperature to block unspecific immunostaining. Embryos were then treated with primary antibodies diluted in 0.1% PBST containing 1% BSA overnight at 4°C inside a moistened chamber. Next morning, embryos were sequentially washed in 0.1% PBST for 5, 15, 20, and 30 min at room temperature. A second blocking was performed in 0.1% PBST containing 3% BSA for 45 min at room temperature. For the secondary staining, embryos were placed in 0.1% PBST containing 1% BSA with the corresponding antibodies and 5 μg/mL of DAPI (D1306, Invitrogen). Embryos were left in secondary staining solution for 90 min at room temperature inside a moistened chamber in the dark. Three washes in 0.1% PBST were performed before mounting the embryos in 10-μL drops of PBS on 35-mm coverglass plates (P35G-1.0-14-C, MatTek) covered in light oil (M5310, Sigma). Embryos were imaged in a Zeiss LSM 980 with Airyscan 2 inverted confocal microscopes and further processed in Fiji and Imaris software for intensity quantifications and distance measurements. Of note, all the incubation steps were performed on shaking platforms.

Mouse ESC culture and infection with C/EBPα

ESCs (E14TG2) were cultured on gelatinized plates in 15% ES-FBS (16141079, Life Technologies) Knockout medium (10829018, Gibco) containing 1,000 U/mL LIF (ESG1106, Merck Millipore). For C/EBPα expression, cells were infected with inducible C/EBPα-ERT2-dTomato lentiviral vector and single-cell clones were expanded after FACS sorting. For C/EBPα induction, cells were treated with 1 μM 4-hydroxytamoxifen (H7904, Sigma), which shuttles the factor into the cell nucleus. The final culture medium also contained 100 U/mL penicillin-100 ng/mL streptomycin, 2 mM L-glutamine, 0.1 mM 2-mercaptoethanol, 100× MEM non-essential amino acid solution, and 1 mM sodium pyruvate.

RNA isolation and RNA-seq

RNA was extracted from B cells and mESCs with a miRNeasy mini kit (217,004, QIAGEN), quantified with a NanoDrop spectrophotometer, and its quality examined in a fragment Bioanalyzer (Aligent 2100 Bioanalyzer DNA 7500 assay). For RNA-seq, libraries were prepared with a TruSeq Stranded mRNA Library Preparation Kit (Illumina) followed by single-end sequencing (50 bp) on an HiSeq 2500 instrument (Illumina), obtaining at least 40 million reads per sample.

For eight-cell embryos and late blastocysts, RNA was extracted and retro-transcribed into cDNA using an SMART-Seq v4 Ultra Low Input RNA kit (634894, Takara). RNA concentration and quality was determined as above. Libraries for RNA-seq were prepared as described previously (Picelli et al., 2014) and sequenced as above.

Computational analyses of RNA-seq data

Reads were mapped using STAR (Dobin et al., 2013) (standard options) and the Ensembl mouse genome annotation version mm10vM21. Gene expression was quantified using STAR (–quantMode GeneCounts). Sample scaling and statistical analysis were performed using the R package DESeq2 (Love et al., 2014) (R 3.3.2 and Bioconductor 3.0). Statistical power of gene expression variation at any given time point was identified using the nbinomLRT test. Log2-vsd (variance stabilized DESeq2) counts were used for further analysis unless stated otherwise. Clustering was performed using the K-means method.

Statistics

Statistical analyses were performed using Prism 9 software. To calculate significance, samples from at least three biologically independent experiments were analyzed. Two biological replicates were used for RNA-seq experiments and statistics applied to the expression of a collection of genes (see Table S1). For samples with $n \geq 3$, values shown in the figures represent median ± SD with 10–90 percentile boxplots and whiskers. One- and two-way ANOVA (with the corresponding multiple comparison analyses) and Student's t tests were applied accordingly. p values appear indicated in each figure.

Data and code availability

The RNA-seq datasets generated and analyzed for the current study are available in the Gene Expression Omnibus (GEO) database under accession numbers GSE202611 for *Il6*$^{-/-}$ and wild-type B cell reprogramming and F1 embryos from *Cebpa*$^{+/-}$ crosses and GSE202613 for the C/EBPα overexpression in mouse ESCs.

SUPPLEMENTAL INFORMATION

Supplemental information can be found online at https://doi.org/10.1016/j.stemcr.2022.07.009.

Data and code availability

The RNA-seq datasets generated and analyzed for the current study are available in the Gene Expression Omnibus (GEO) database under accession numbers GSE202611 for *Il6*$^{-/-}$ and wild-type B cell reprogramming and F1 embryos from *Cebpa*$^{+/-}$ crosses and GSE202613 for the C/EBPα overexpression in mouse ESCs.

AUTHOR CONTRIBUTIONS

M.P.-C. and T.G. conceived the study and wrote the manuscript. M.P.-C. performed reprogramming, transdifferentiation, pre-implantation embryo manipulation, molecular biology RNA-seq experiments, and analyzed the data. G.S. and M.V.-C. processed ChIP-seq, RNA-seq, and ATAC-seq data. R.B., C.D.R.W., A.K., and M.F. analyzed single-cell expression data. C.S.-M. performed western blot and immunostaining experiments. N.A. provided bones from *Il6*$^{-/-}$ mice. L.d.A.-A. produced recombinant proteins in conditioned medium. M.G. and N.P. injected mRNA constructs and imaged mouse embryos. T.V.T. and G.T.G. performed RNA-seq experiments. M.S. provided invaluable advice and T.G. supervised the research.

ACKNOWLEDGMENTS

We thank C. Berenguer for help with B cell reprogramming and bone marrow collection; S. Nakagawa and B. Pernaute for advice on pre-implantation embryo culture and manipulation, and Kyle M. Loh for his valuable discussions; the flow cytometry and microscopy units of UPF-CRG for technical assistance; the CRG genomics core facility for sequencing and Graf laboratory members for critical discussions. Work in the laboratory of T.G. was supported by the Spanish Ministry of Economy, Industry and Competitiveness (Plan Estatal PID2019-109354GB-I00), the CRG, AGAUR (SGR 726), and a European Research Council Synergy grant (4D-Genome). M.P.-C. was supported by an FPI fellowship (BES-2016-076900). Work in the laboratory of M.S. was funded by the IRB and by grants from the Spanish Ministry of Economy co-funded by the European Regional Development Fund (SAF2017-82613-R), ERC (ERC-2014-AdG/669622), la Caixa Foundation, and Secretaria d'Universitats i Recerca del Departament d'Empresa i Coneixement of Catalonia (Grup de Recerca consolidat 2017 SGR 282).

CONFLICTS OF INTEREST

The authors declare no competing interests.

Received: May 23, 2022
Revised: July 14, 2022
Accepted: July 14, 2022
Published: August 11, 2022

SUPPORTING CITATIONS

The following references appear in the supplemental information: Bussmann et al. (2009); Carey et al. (2010); Labbé et al. (2012).

REFERENCES

Abad, M., Mosteiro, L., Pantoja, C., Cañamero, M., Rayon, T., Ors, I., Graña, O., Megías, D., Domínguez, O., Martínez, D., et al. (2013). Reprogramming in vivo produces teratomas and iPS cells with totipotency features. Nature *502*, 340–345. https://doi.org/10.1038/nature12586.

Akira, S., Isshiki, H., Sugita, T., Tanabe, O., Kinoshita, S., Nishio, Y., Nakajima, T., Hirano, T., and Kishimoto, T. (1990). A nuclear factor for IL-6 expression (NF-IL6) is a member of a C/EBP family. EMBO J *9*, 1897–1906. https://doi.org/10.1002/j.1460-2075.1990.tb08316.x.

Bourillot, P.Y., Santamaria, C., David, L., and Savatier, P. (2020). GP130 signaling and the control of naïve pluripotency in humans, monkeys, and pigs. Exp. Cell Res. *386*, 111712. https://doi.org/10.1016/j.yexcr.2019.111712.

Brady, J.J., Li, M., Suthram, S., Jiang, H., Wong, W.H., and Blau, H.M. (2013). Early role for IL-6 signalling during generation of induced pluripotent stem cells revealed by heterokaryon RNA-Seq. Nat. Cell Biol. *15*, 1244–1252. https://doi.org/10.1038/ncb2835.

Bussmann, L.H., Schubert, A., Vu Manh, T.P., Desbordes, S.C., Parra, M., Zimmermann, T., Rapino, F., et al. (2009). A robust and highly efficient immune cell reprogramming system. Cell Stem Cell *5*, 554–566. https://doi.org/10.1016/j.stem.2009.10.004.

Carey, B.W., Markoulaki, S., Beard, C., Hanna, J., and Jaenisch, R. (2010). Single-gene transgenic mouse strains for reprogramming adult somatic cells. Nat. Methods *7*, 56–59. https://doi.org/10.1038/NMETH.1410.

Chiche, A., Le Roux, I., von Joest, M., Sakai, H., Aguín, S.B., Cazin, C., Salam, R., Fiette, L., Alegria, O., Flamant, P., et al. (2017). Injury-induced senescence enables in vivo reprogramming in skeletal muscle. Cell Stem Cell *20*, 407–414.e4. https://doi.org/10.1016/j.stem.2016.11.020.

Deng, Q., Ramsköld, D., Reinius, B., and Sandberg, R. (2014). Single-cell RNA-seq reveals dynamic, random monoallelic gene expression in mammalian cells. Science *343*, 193–196. https://doi.org/10.1126/science.1245316.

Di Stefano, B., Sardina, J.L., van Oevelen, C., Collombet, S., Kallin, E.M., Vicent, G.P., Lu, J., Thieffry, D., Beato, M., and Graf, T. (2014). C/EBPα poises B cells for rapid reprogramming into induced pluripotent stem cells. Nature *506*, 235–239. https://doi.org/10.1038/nature12885.

Di Stefano, B., Collombet, S., Jakobsen, J.S., Wierer, M., Sardina, J.L., Lackner, A., Stadhouders, R., Segura-Morales, C., Francesconi, M., Limone, F., et al. (2016). C/EBPα creates elite cells for iPSC reprogramming by upregulating Klf4 and increasing the levels of Lsd1 and Brd4. Nat. Cell Biol. *18*, 371–381. https://doi.org/10.1038/ncb3326.

Do, D.V., Ueda, J., Messerschmidt, D.M., Lorthongpanich, C., Zhou, Y., Feng, B., Guo, G., Lin, P.J., Hossain, M.Z., Zhang, W., et al. (2013). A genetic and developmental pathway from STAT3 to the OCT4-NANOG circuit is essential for maintenance of ICM lineages in vivo. Genes Dev. *27*, 1378–1390. https://doi.org/10.1101/gad.221176.113.

Dobin, A., Davis, C.A., Schlesinger, F., Drenkow, J., Zaleski, C., Jha, S., Batut, P., Chaisson, M., and Gingeras, T.R. (2013). STAR: ultrafast universal RNA-seq aligner. Bioinformatics *29*, 15–21. https://doi.org/10.1093/bioinformatics/bts635.

Eminli, S., Foudi, A., Stadtfeld, M., Maherali, N., Ahfeldt, T., Mostoslavsky, G., Hock, H., and Hochedlinger, K. (2009). Differentiation stage determines potential of hematopoietic cells for reprogramming into induced pluripotent stem cells. Nat. Genet. *41*, 968–976. https://doi.org/10.1038/ng.428.

Francesconi, M., Di Stefano, B., Berenguer, C., de Andrés-Aguayo, L., Plana-Carmona, M., Mendez-Lago, M., Guillaumet-Adkins, A., Rodriguez-Esteban, G., Gut, M., Gut, I.G., et al. (2019). Single cell RNA-seq identifies the origins of heterogeneity in efficient cell transdifferentiation and reprogramming. Elife *8*. e41627–22. https://doi.org/10.7554/eLife.41627.

Gardner, R.L. (2000). Flow of cells from polar to mural trophectoderm is polarized in the mouse blastocyst. Hum. Reprod. *15*, 694–701. https://doi.org/10.1093/humrep/15.3.694.

Graf, T. (2011). Historical origins of transdifferentiation and reprogramming. Cell Stem Cell *9*, 504–516. https://doi.org/10.1016/j.stem.2011.11.012.

Guo, G., Huss, M., Tong, G.Q., Wang, C., Li, Sun L., Clarke, N.D., and Robson, P. (2010). Resolution of cell fate decisions revealed by single-cell gene expression analysis from zygote to blastocyst. Dev. Cell *18*, 675–685. https://doi.org/10.1016/j.devcel.2010.02.012.

Guo, S., Zi, X., Schulz, V.P., Cheng, J., Zhong, M., Koochaki, S.H.J., Megyola, C.M., Pan, X., Heydari, K., Weissman, S.M., et al. (2014). Nonstochastic reprogramming from a privileged somatic cell state. Cell *156*, 649–662. https://doi.org/10.1016/j.cell.2014.01.020.

Guo, G., Stirparo, G.G., Strawbridge, S.E., Spindlow, D., Yang, J., Clarke, J., Dattani, A., Yanagida, A., Li, M.A., Myers, S., et al. (2021). Human naive epiblast cells possess unrestricted lineage potential. Cell Stem Cell *28*, 1040–1056.e6. https://doi.org/10.1016/j.stem.2021.02.025.

Hunter, C.A., and Jones, S.A. (2015). IL-6 as a keystone cytokine in health and disease. Nat. Immunol. *16*, 448–457. https://doi.org/10.1038/ni.3153.

Kopf, M., Baumann, H., Freer, G., Freudenberg, M., Lamers, M., Kishimoto, T., Zinkernagel, R., Bluethmann, H., and Köhler, G. (1994). Impaired immune and acute-phase responses in interleukin-6-deficient mice. Nature *368*, 339–342. https://doi.org/10.1038/368339a0.

Krendl, C., Shaposhnikov, D., Rishko, V., Ori, C., Ziegenhain, C., Sass, S., Simon, L., Müller, N.S., Straub, T., Brooks, K.E., et al. (2017). GATA2/3-TFAP2A/C transcription factor network couples human pluripotent stem cell differentiation to trophectoderm with repression of pluripotency. Proc. Natl. Acad. Sci. USA *114*, E9579–E9588. https://doi.org/10.1073/pnas.1708341114.

Kuilman, T., Michaloglou, C., Vredeveld, L.C.W., Douma, S., van Doorn, R., Desmet, C.J., Aarden, L.A., Mooi, W.J., and Peeper,

D.S. (2008). Oncogene-induced senescence relayed by an interleukin-dependent inflammatory network. Cell *133*, 1019–1031. https://doi.org/10.1016/j.cell.2008.03.039.

Labbé, R.M., Irimia, M., Currie, K.W., Lin, A., Zhu, S.J., Brown, D.D.R., Ross, E.J., Voisin, V., Bader, G.D., Blencowe, B.J., and Pearson, B.J. (2012). A Comparative transcriptomic analysis reveals conserved features of stem cell pluripotency in planarians and mammals. Stem Cell. *30*, 1734–1745. https://doi.org/10.1002/stem.1144.

Li, R., Liang, J., Ni, S., Zhou, T., Qing, X., Li, H., He, W., Chen, J., Li, F., Zhuang, Q., et al. (2010). A mesenchymal-to-Epithelial transition initiates and is required for the nuclear reprogramming of mouse fibroblasts. Cell Stem Cell *7*, 51–63. https://doi.org/10.1016/j.stem.2010.04.014.

Liu, X., Ouyang, J.F., Rossello, F.J., Tan, J.P., Davidson, K.C., Valdes, D.S., Schröder, J., Sun, Y.B.Y., Chen, J., Knaupp, A.S., et al. (2020). Reprogramming roadmap reveals route to human induced trophoblast stem cells. Nature *586*, 101–107. https://doi.org/10.1038/s41586-020-2734-6.

Love, M.I., Huber, W., and Anders, S. (2014). Moderated estimation of fold change and dispersion for RNA-seq data with DESeq2. Genome Biol. *15*, 550–621. https://doi.org/10.1186/s13059-014-0550-8.

Mackey, S.L., and Darlington, G.J. (2004). CCAAT enhancer-binding protein α is required for interleukin-6 receptor α signaling in newborn hepatocytes. J. Biol. Chem. *279*, 16206–16213. https://doi.org/10.1074/jbc.M400737200.

Mosteiro, L., Pantoja, C., Alcazar, N., Marión, R.M., Chondronasiou, D., Rovira, M., Fernandez-Marcos, P.J., Muñoz-Martin, M., Blanco-Aparicio, C., Pastor, J., et al. (2016). Tissue damage and senescence provide critical signals for cellular reprogramming in vivo. Science *354*, aaf4445. https://doi.org/10.1126/science.aaf4445.

Nakamura, T., Yabuta, Y., Okamoto, I., Aramaki, S., Yokobayashi, S., Kurimoto, K., Sekiguchi, K., Nakagawa, M., Yamamoto, T., and Saitou, M. (2015). SC3-seq: a method for highly parallel and quantitative measurement of single-cell gene expression. Nucleic Acids Res. *43*, e60. https://doi.org/10.1093/nar/gkv134.

Nakatake, Y., Ko, S.B.H., Sharov, A.A., Wakabayashi, S., Murakami, M., Sakota, M., Chikazawa, N., Ookura, C., Sato, S., Ito, N., et al. (2020). Generation and profiling of 2, 135 human ESC lines for the systematic analyses of cell states perturbed by inducing single transcription factors. Cell Rep. *31*, 107655. https://doi.org/10.1016/j.celrep.2020.107655.

Petropoulos, S., Edsgärd, D., Reinius, B., Deng, Q., Panula, S.P., Codeluppi, S., Plaza Reyes, A., Linnarsson, S., Sandberg, R., and Lanner, F. (2016). Single-cell RNA-seq reveals lineage and X chromosome dynamics in human preimplantation embryos. Cell *165*, 1012–1026. https://doi.org/10.1016/j.cell.2016.03.023.

Picelli, S., Faridani, O.R., Björklund, A.K., Winberg, G., Sagasser, S., and Sandberg, R. (2014). Full-length RNA-seq from single cells using Smart-seq2. Nat. Protoc. *9*, 171–181. https://doi.org/10.1038/nprot.2014.006.

Rivron, N.C., Frias-Aldeguer, J., Vrij, E.J., Boisset, J.C., Korving, J., Vivié, J., Truckenmüller, R.K., van Oudenaarden, A., van Blitterswijk, C.A., and Geijsen, N. (2018). Blastocyst-like structures generated solely from stem cells. Nature *557*, 106–111. https://doi.org/10.1038/s41586-018-0051-0.

Rossant, J., and Tam, P.P.L. (2022). Early human embryonic development: blastocyst formation to gastrulation. Dev. Cell *57*, 152–165. https://doi.org/10.1016/j.devcel.2021.12.022.

Schiebinger, G., Shu, J., Tabaka, M., Cleary, B., Subramanian, V., Solomon, A., Gould, J., Liu, S., Lin, S., Berube, P., et al. (2019). Optimal-transport analysis of single-cell gene expression identifies developmental trajectories in reprogramming. Cell *176*, 928–943.e22. https://doi.org/10.1016/j.cell.2019.01.006.

Sellens, M.H., and Jenkinson, E.J. (1975). Permeability of the mouse zona pellucida to immunoglobulin. J. Reprod. Fertil. *42*, 153–157. https://doi.org/10.1530/jrf.0.0420153.

Shen, X.H., Cui, X.S., Lee, S.H., and Kim, N.H. (2012). Interleukin-6 enhances porcine parthenote development in vitro, through the IL-6/Stat3 signaling pathway. J. Reprod. Dev. *58*, 453–460. https://doi.org/10.1262/jrd.2012-015.

Stik, G., Vidal, Enrique, Barrero, Mercedes, Cuartero, Sergi, Vila-Casadesús, Maria, Mendieta-Esteban, Julen, Tian, Tian V., et al. (2020). CTCF is dispensable for immune cell transdifferentiation but facilitates an acute inflammatory response. Nat. Genet. *52*, 655–661. https://doi.org/10.1038/s41588-020-0643-0.

Von Laue, S., Finidori, J., Maamra, M., Shen, X.Y., Justice, S., Dobson, P.R., and Ross, R.J. (2000). Stimulation of endogenous GH and interleukin-6 receptors selectively activates different Jaks and Stats, with a Stat5 specific synergistic effect of dexamethasone. J. Endocrinol. *165*, 301–311. https://doi.org/10.1677/joe.0.1650301.

Wang, N.D., Finegold, M.J., Bradley, A., Ou, C.N., Abdelsayed, S.V., Wilde, M.D., Taylor, L.R., Wilson, D.R., and Darlington, G.J. (1995). Impaired energy homeostasis in C/EBPα knockout mice. Science *269*, 1108–1112. https://doi.org/10.1126/science.7652557.

Wooldridge, L.K., and Ealy, A.D. (2019). Interleukin-6 increases inner cell mass numbers in bovine embryos. BMC Dev. Biol. *19*, 2–11. https://doi.org/10.1186/s12861-019-0182-z.

Xie, H., Ye, M., Feng, R., and Graf, T. (2004). Stepwise reprogramming of B cells into macrophages. Cell *117*, 663–676.

Zhang, D.E., Zhang, P., Wang, N.D., Hetherington, C.J., Darlington, G.J., and Tenen, D.G. (1997). Absence of granulocyte colony-stimulating factor signaling and neutrophil development in CCAAT enhancer binding protein α-deficient mice. Proc. Natl. Acad. Sci. USA *94*, 569–574. https://doi.org/10.1073/pnas.94.2.569.

Zhu, M., and Zernicka-Goetz, M. (2020). Principles of self-organization of the mammalian embryo. Cell *183*, 1467–1478. https://doi.org/10.1016/j.cell.2020.11.003.